

On the effective measurement frequency of time domain reflectometry in dispersive and nonconductive dielectric materials

D. A. Robinson,¹ M. G. Schaap,² D. Or,³ and S. B. Jones¹

Received 16 November 2004; accepted 4 December 2004; published 5 February 2005.

[1] Time domain reflectometry (TDR) is one of the most commonly used techniques for water content determination in the subsurface. The measurement results in a single bulk permittivity value that corresponds to a particular, but unknown, “effective” frequency (f_{eff}). Estimating f_{eff} using TDR is important, as it allows comparisons with other techniques, such as impedance or capacitance probes, or microwave remote sensing devices. Soils, especially those with high clay and organic matter content, show appreciable dielectric dispersion, i.e., the real permittivity changes as a function of frequency. Consequently, comparison of results obtained with different sensor types must account for measurement frequency in assessing sensor accuracy and performance. In this article we use a transmission line model to examine the impact of dielectric dispersion on the TDR signal, considering lossless materials (negligible electrical conductivity). Permittivity is inferred from the standard tangent line fitting procedure (K_{aTAN}) and by a method of using the apex of the derivative of the TDR waveform (K_{aDER}). The permittivity determined using the tangent line method is considered to correspond to a velocity associated with a maximum passable frequency; whereas we consider the permittivity determined from the derivative method to correspond with the frequency associated with the signal group velocity. The effective frequency was determined from the 10–90% risetime of the reflected signal. On the basis of this definition, f_{eff} was found to correspond with the permittivity determined from K_{aDER} and not from K_{aTAN} in dispersive dielectrics. The modeling is corroborated by measurements in bentonite, ethanol and 1-propanol/water mixtures, which demonstrate the same result. Interestingly, for most nonconductive TDR measurements, frequencies are expected to lie in a range from 0.7 to 1 GHz, while in dispersive media, f_{eff} is expected to fall below 0.6 GHz.

Citation: Robinson, D. A., M. G. Schaap, D. Or, and S. B. Jones (2005), On the effective measurement frequency of time domain reflectometry in dispersive and nonconductive dielectric materials, *Water Resour. Res.*, 41, W02007, doi:10.1029/2004WR003816.

1. Introduction

[2] Time domain reflectometry is a standard method for determining water content in soils and other porous media [Topp *et al.*, 1980; Topp and Ferre, 2002; Robinson *et al.*, 2003a]. It is one of a number of techniques that use the dielectric properties of soil, sediments and rocks to determine water content. Other techniques include capacitance probes [Dean *et al.*, 1987; Paltineanu and Starr, 1997; Kelleners *et al.*, 2004], ground penetrating radar [Huisman *et al.*, 2003] and active microwave remote sensing [McNairn *et al.*, 2002]. All of these techniques operate at different frequencies, and when the permittivity of a soil is not affected by bulk electrical conductivity and does not change considerably with frequency, measurements made

with differing techniques may be compared. However, clay minerals have been shown to exhibit dielectric dispersion to differing extents [Fernando *et al.*, 1977]. This means that the real (ϵ') and imaginary (ϵ'') parts of the permittivity describing energy storage and energy losses respectively, change as a function of frequency. In general, kaolinite exhibits the lowest dispersion, montmorillonite shows the highest with illite being somewhat intermediate [Fernando *et al.*, 1977]. This means that some water bearing earth materials, especially clay soils may show dielectric dispersion. When this is the case, and measurements are to be compared, it is important to know the frequency to which a permittivity determination corresponds.

[3] Several studies in the literature have aimed at determining and using an “effective frequency” for the TDR measurement [Hilhorst, 1998; Sun *et al.*, 2000; Topp *et al.*, 2000; Hook *et al.*, 2004]. Two methods have been presented, the first, a more pragmatic method that compares the measured value of permittivity obtained from fitting tangent lines to the waveform, with the permittivity obtained from the frequency domain dispersion curve [Or and Rasmussen, 1999; Robinson *et al.*, 2003a]. The assumption is made that the imaginary permittivity is small and that $K_a \approx \epsilon'$. The

¹Department of Plants, Soils and Biometeorology, Utah State University, Logan, Utah, USA.

²George E. Brown Jr. Salinity Laboratory, Riverside, California, USA.

³Department of Civil and Environmental Engineering, University of Connecticut, Storrs, Connecticut, USA.

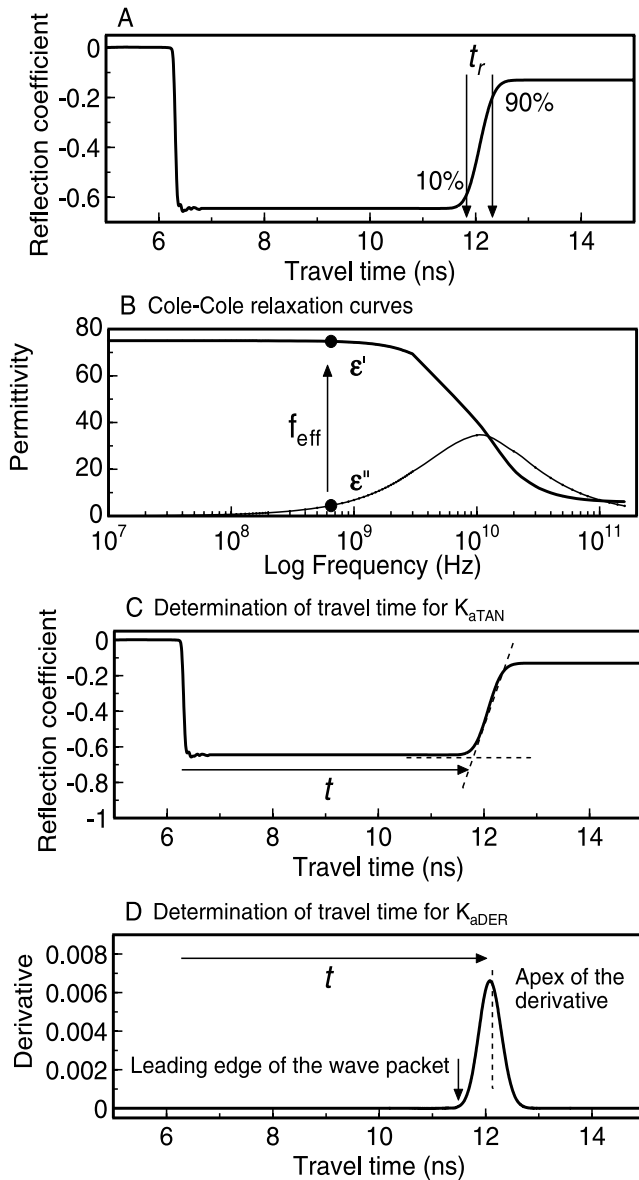


Figure 1. Graphical description of the procedure followed to obtain frequency and apparent permittivity. (a) Determination of risetime, t_r , from the TDR waveform using the 10–90% values, where t_r is used in equation (1) to determine frequency. (b) Effective frequency. Corresponding values of ϵ' and ϵ'' are determined from the *Debye* [1929] curve. These values are fed into equation (3) to determine the apparent permittivity K_a . (c) Waveform where travel time (t) is determined according to the tangent line fitting procedure from which K_{aTAN} is determined. (d) Derivative of the waveform in Figure 1c. Travel time (t) is correlated with the apex of the derivative for K_{aDER} determination. Finally, these values are plotted against K_a determined from the effective frequency and are shown in the results as Figure 3.

point at which the two values coincide is used to estimate the “maximum passable frequency” for the measurement. The second method is derived from a more theoretical approach based on the description in Appendix C of the Tektronix application note entitled “TDR’s for cable

testing” (J. A. Strickland, Time-domain reflectometry measurements, pp. 11–13, Tektronix Inc., Beaverton, Oregon, 1970). This method uses the risetime of the reflected signal to determine the effective frequency (Figure 1a). Given the value of t_r (Figure 1) the effective frequency is calculated according to J. A. Strickland (Time-domain reflectometry measurements, pp. 11–13, Tektronix Inc., Beaverton, Oregon, 1970). as

$$f_{eff} = \frac{\ln \left[\frac{0.9}{0.1} \right]}{2\pi t_r} \quad (1)$$

This simplifies to $f_{eff}(\text{Hz}) = 0.35/t_r$, where t_r is measured in seconds. This method has been applied in a number of studies [Hilhorst, 1998; Sun *et al.*, 2000; Topp *et al.*, 2000; Hook *et al.*, 2004]; however, different definitions of risetime are used. The problem considered in this paper is to determine which method of determining permittivity, tangent line or apex of the derivative, agrees with the effective frequency determined using equation (1). In so doing TDR permittivity measurements can be matched to an effective frequency and compared with either other instruments or soil dielectric spectra. In previous work [Topp *et al.*, 2000] the frequency determined using equation (1) has been considered to correspond with the permittivity measured from travel time determined by fitting tangent lines to the TDR waveform. The aim of this paper is to demonstrate, through TDR waveform modeling, that this is incorrect for dispersive dielectric media. The effective frequency determined in this manner corresponds to the permittivity determined from the apex of the derivative of the waveform of the reflected signal. This will be accomplished by first considering computed waveforms for a range of permittivities and relaxation frequencies that are indeterminate from experiment. After which we will demonstrate the validity of our analysis with water/1-propanol mixtures as a dispersive soil/sediment simulant.

2. Theoretical Considerations

2.1. Apparent Permittivity Measured Using TDR

[4] TDR measures the propagation velocity of a step voltage pulse that has a wide bandwidth, usually 20 kHz to 1.5 GHz [Heimovaara, 1994], and thus the velocity of this signal is primarily a function of the permittivity of the material through which it travels. The relationship between the velocity of the signal, and the dielectric properties of the medium through which it travels, can be understood using the analogy of the phase velocity (v_{phase}) of a sinusoidal plane wave along a transmission line:

$$v_{phase} = \frac{1}{\sqrt{\mu_o \mu_r \epsilon_o \epsilon_r}} = \frac{c}{\sqrt{\mu_r \epsilon_r}} \quad (2)$$

where c is the velocity of light ($3 \times 10^8 \text{ ms}^{-1}$), ϵ_r is the relative permittivity, μ_o is the permeability of vacuum ($1.257 \times 10^{-6} \text{ H}$) and μ_r is the relative magnetic permeability. The velocity of the signal in a nonmagnetic, nondispersive, nonconductive dielectric is hence $v_{phase} = (2l/t)$ where l is the length of the TDR probe in meters and t is the total TDR reflection (back and forth along the probe),

and $v_{\text{phase}} = (c/\sqrt{\epsilon_r})$. Therefore by equating both of these and rearranging gives the round trip propagation time (t) of the wave as a function of both the length of transmission line (l) and the permittivity of the material, $t = [(2l\sqrt{\epsilon_r})/c]$. Hence it follows that the permittivity can be determined by measuring the time it takes the wave to traverse the probe. However, in a dispersive dielectric medium where both the real and imaginary permittivity changes with frequency the TDR measures an apparent permittivity K_a . This apparent permittivity can be described using an analogy for a sinusoidal plane wave [Von Hippel, 1954]:

$$K_a = \frac{\epsilon'(\omega)}{2} \left[1 + \sqrt{1 + \left[\left(\epsilon''(\omega) + \frac{\sigma_{dc}}{\omega\epsilon_o} \right) / (\epsilon'(\omega)) \right]^2} \right] \quad (3)$$

where K_a is the measured apparent permittivity, ϵ' is the real part of the permittivity due to energy storage and ϵ'' is the imaginary component due to losses [White *et al.*, 1994], ω represents the angular frequency $2\pi f$, where f is the frequency in Hz. Hilhorst [1998] has raised doubts about using this equation as it is only an analogy that is derived from the propagation constant of an EM sine wave. However, it remains a useful analogy until more, nontrivial theoretical work is done to develop a more robust model. According to Hilhorst [1998], this would use the Telegrapher's equations [Wadell, 1991] to work out the response of a step function in the time domain.

[5] Traditional waveform analysis, dating to Topp *et al.*'s [1980] seminal work, has used the fitting of tangent lines to the waveform reflection to determine travel time, as demonstrated in Figure 1c. Tangent lines are fitted to the waveform reflection and the travel time is traditionally calculated from the point corresponding to ~ 6.5 ns to the point at which the tangent lines intersect (~ 11.8 ns). This travel time corresponds to the signal phase velocity. In this work we argue that it is more appropriate to consider the derivative of the waveform (Figure 1d). In this case the travel time is determined from the start point to the points marked, apex of the derivative. The reason that this is done is that the signals are now viewed as wave packets [Elmore and Heald, 1985], the apex of which should correspond to the maximum energy density of the wave packet. Travel time determined from the apex of the derivative corresponds with the group velocity of the signal. In dispersive media it is more appropriate to determine permittivity from the group velocity, at which the energy travels, rather than the phase velocity which represents the leading edge of the wave packet where there is minimal energy.

[6] Water content is then determined using the permittivity from the TDR waveform analysis. This can be achieved using an empirical approach such as the Topp equation [Topp *et al.*, 1980] which has been successfully applied to many coarse textured soils. Alternatively dielectric mixing models can be used such as those used by Dirksen and Dasberg [1993].

2.2. TDR Waveform Modeling

2.2.1. TDR Response Function

[7] Analysis and modeling of TDR waveforms is most easily and efficiently done in the frequency domain by convolution of an input signal, V_o , with the S_{11} scatter function that contains all the relevant electromagnetic prop-

erties of the cable-probe system. The response function R at frequency f is calculated as

$$R(f) = V_o(f)S_{11}(f) \quad (4)$$

A relatively clean input signal, $V_o(f)$, can be determined by using a procedure outlined by Huisman *et al.* [2002]. In this approach, open and short-circuited time domain waveforms ($W_o(t)$ and $W_s(t)$) were measured by connecting standard open and short calibration loads (Model 8550Q, Maury Microwave Corporation, Ontario, California) to the port of the cable tester. A waveform, $W(t)$, with minimal internal reflections is then computed by

$$W(t) = (W_o(t) - W_s(t))/2 \quad (5)$$

The $W_o(t)$ and $W_s(t)$ signals were acquired with a program developed by Heimovaara [1994] that was modified to measure 16,384 points from -0.5 m to approximately 65 meters with the propagation speed setting of the Tek1502B at 0.99. The input signal $V_o(f)$ was computed by taking the back difference of $W(t)$, followed by a fast Fourier transform [Heimovaara, 1994]. The input signal ranges from 0 to 37.1150 GHz, in steps of 4.5312 MHz. Inspection of the spectrum, however, indicates that the signal does not contain relevant information beyond 6 GHz (results not shown).

2.2.2. Composite Scatter Function for a Segmented Probe

[8] Heimovaara [1994] used a special 7-wire probe configuration that required only the scatter function of the sensor to be known. In this study we consider a probe that consists of two segments, a 50 ohm cable of 1m length, and a 0.2 m coaxial TDR probe, each with a separate scatter function. The diameter of the inner electrode being, 6.35 mm and the outer electrode, 25.4 mm. Feng *et al.* [1999] showed how to compute effective scatter functions for such segmented systems. In essence their theory involves determining the impedances, propagation constants, and reflection coefficients for individual segments, after which the effective scatter function can be computed following Feng *et al.* [1999]:

$$S_{11}^k(f) = \frac{\rho_s^k(f) + S_{11}^{k+1}(f)H^k(f, 2L_s^k)}{1 + \rho_s^k(f)S_{11}^{k+1}(f)H^k(f, 2L_s^k)} \quad (6)$$

where k is the segment number, ranging from 1 (the first segment in the probe) to the number of segments N , $\rho_s^k(f)$ is the reflection coefficient (equation (6)) and H is the propagation function (equation (8)). Equation (6) is recursive, meaning that in order to compute the scatter function for the entire system (i.e., $k = 1$) it is necessary to subsequently compute the $S_{11}^k(f)$ for $k = N, N - 1, \dots, 3, 2$, and finally 1. The scatter function for $k = N$ is computed by setting $S_{11}^{N+1}(f)$ equal to the end reflection, which is 1 and -1 for open-ended and shorted probes, respectively [Feng *et al.*, 1999; Schaap *et al.*, 2003]. The reflection coefficient $\rho_s^k(f)$ is computed according to Feng *et al.* [1999]:

$$\rho_s^k = \frac{Z_{k-1}(f) - Z_k(f)}{Z_{k-1}(f) + Z_k(f)} \quad (7)$$

where $Z_k(f)$ is the impedance for segment k at frequency f ; Z_0 is equal to the impedance of the cable that is attached to

the probe, in our case 50 ohm. The propagation function $H^k(f, x)$ is computed according to

$$H(f, x) = e^{-\gamma x} \quad (8)$$

where x is a place holder for the segment length (L_s in equation (6)) and γ is the propagation constant which is computed as:

$$\gamma = \sqrt{(i2\pi fL + R_s)(i2\pi fC + G)} \quad (9)$$

where i denotes a complex quantity $\sqrt{-1}$, and L and C are the inductance and capacitance of the segment, respectively. R_s and G are the skin resistance of the conductor and the conductance of the medium, respectively. For the purposes of this study, both will be set to zero.

[9] The quantities Z , L and C are dependent on the magnetic (L) and dielectric properties (C) of the medium and also depend on the geometry of the probe. For coaxial probes the following expressions hold [Ibbotson, 1999]:

$$L = \frac{\mu_r}{2\pi} \ln(b/a) \quad (\text{H/m}) \quad (10)$$

$$C = \frac{2\pi\epsilon_r}{\ln(b/a)} \quad (\text{F/m}) \quad (11)$$

$$Z = \sqrt{L/C} = \frac{\ln(b/a)}{2\pi} \sqrt{\frac{\mu_r}{\epsilon_r}} \quad (12)$$

where b is the diameter of the outer conductor, and a is the diameter of the inner conductor. The medium we studied had no magnetic properties and we therefore set the relative magnetic permeability, μ_r , to unity. Because of the relaxation of the input the complex dielectric permittivity, ϵ^* , is frequency-dependent and was computed with the Debye [1929] equation:

$$\epsilon^* = \epsilon_\infty + \frac{\epsilon_s - \epsilon_\infty}{1 + if/f_{rel}} \quad (13)$$

where ϵ_s and ϵ_∞ are the static permittivity and permittivity at infinite frequency, respectively, f_{rel} is the relaxation frequency.

3. Methods

3.1. Procedure

[10] We simulated waveforms assuming bulk permittivity values of 10, 25, 50, 75 and 100, and infinite frequency permittivity values of 1.44, 2.18, 3.40, 4.63 and 5.85, respectively. We used the Debye [1929] model (equation (13)) to describe the frequency-dependent permittivity and systematically varied the relaxation frequency from 0.001 GHz through, 0.005, 0.01, 0.05, 0.1, 0.5, 1, 5, 10, 50 to 100 GHz. This resulted in 55 waveforms that were each individually analyzed; the analysis steps are presented in Figure 1. Effective length was determined for both K_{aTAN} and K_{aDER} for the probe using waveforms with a real permittivity of 1 and 100. Relaxation was removed so that the effective lengths were determined only as a function of

the real permittivity. The effective length was determined to be 0.200 m using both methods.

[11] 1. Determine the effective frequency from equation (1).

[12] 2. Take this frequency and determine the corresponding real (ϵ') and imaginary (ϵ'') permittivity values from the Debye relaxation curve (Figure 1b). These values of ϵ' and ϵ'' were then inserted into equation (3) to determine the apparent permittivity K_a .

[13] 3. Determine the apparent permittivity from the waveform using tangent line fitting (Figure 1c). This value of apparent permittivity is represented as K_{aTAN} .

[14] 4. Determine the apparent permittivity from the apex of the derivative of the waveform (Figure 1d). This value of apparent permittivity is represented as K_{aDER} .

[15] 5. Plot K_{aTAN} and K_{aDER} against K_a determined using equation (3) from step 2.

3.2. Measurements Using Materials and Liquids

[16] Materials were chosen initially to demonstrate the effective frequency in dielectric liquids with no dispersion. Air (1), oil (3.0), acetone and oil (10.0), acetone (22.7) acetone and water (52.4) and water (78.5) were chosen for this purpose. Two types of dielectrics were then chosen to illustrate how the effective frequency is affected when dispersion increases as a function of permittivity and decreases as a function of permittivity. We used sodium bentonite clay to demonstrate increasing dispersion as a function of permittivity (water content). Measurements were made on repacked samples that were wetted and mixed using an atomizer spray. The measurements were conducted at water contents from air dry ($0.08 \text{ m}^3 \text{ m}^{-3}$) to a water content of about $0.3 \text{ m}^3 \text{ m}^{-3}$; this represents hydration with about 3 layers of water between the clay layers [Chou Chang *et al.*, 1995]. By keeping to water contents below $0.3 \text{ m}^3 \text{ m}^{-3}$ bulk electrical conductivity was minimized and prevented from interfering with the determination of effective frequency from risetime. Water/1-propanol and water-ethanol mixtures were used to demonstrate how a dispersion that reduces as a function of frequency affects the effective frequency. The 1-propanol we used had a permittivity ~ 21 and a relaxation frequency around 0.59 GHz, the ethanol had a permittivity of ~ 29 and a relaxation frequency around 1.38 GHz. Using liquids in preference to powders overcomes a number of experimental uncertainties, these include the liquid being a homogeneous dielectric and packing uniformly within the cell. Measurements were conducted in a coaxial cell, 47 mm in diameter with an inner electrode 1.5 mm in diameter in order to minimize any electrical conductivity affects. The cell was 20 cm long and attached to a 50 cm cable. The cell was calibrated for effective length using air and water [Robinson *et al.*, 2003b]. Nine mixtures of 1-propanol and water were mixed and 11 of water and ethanol to provide a range of permittivity values and relaxation times. Measurements were made with the cell attached to a Tektronix (1502B) cable tester (Tektronix, Beaverton, OR). Waveforms were collected using the software of Heimovaara and de Water [1993] and interpreted manually to obtain (1) the permittivity from tangent line fitting (K_{aTAN}), (2) the permittivity from the apex of the derivative (K_{aDER}), and (3) the effective frequency (f_{eff}), from risetime.

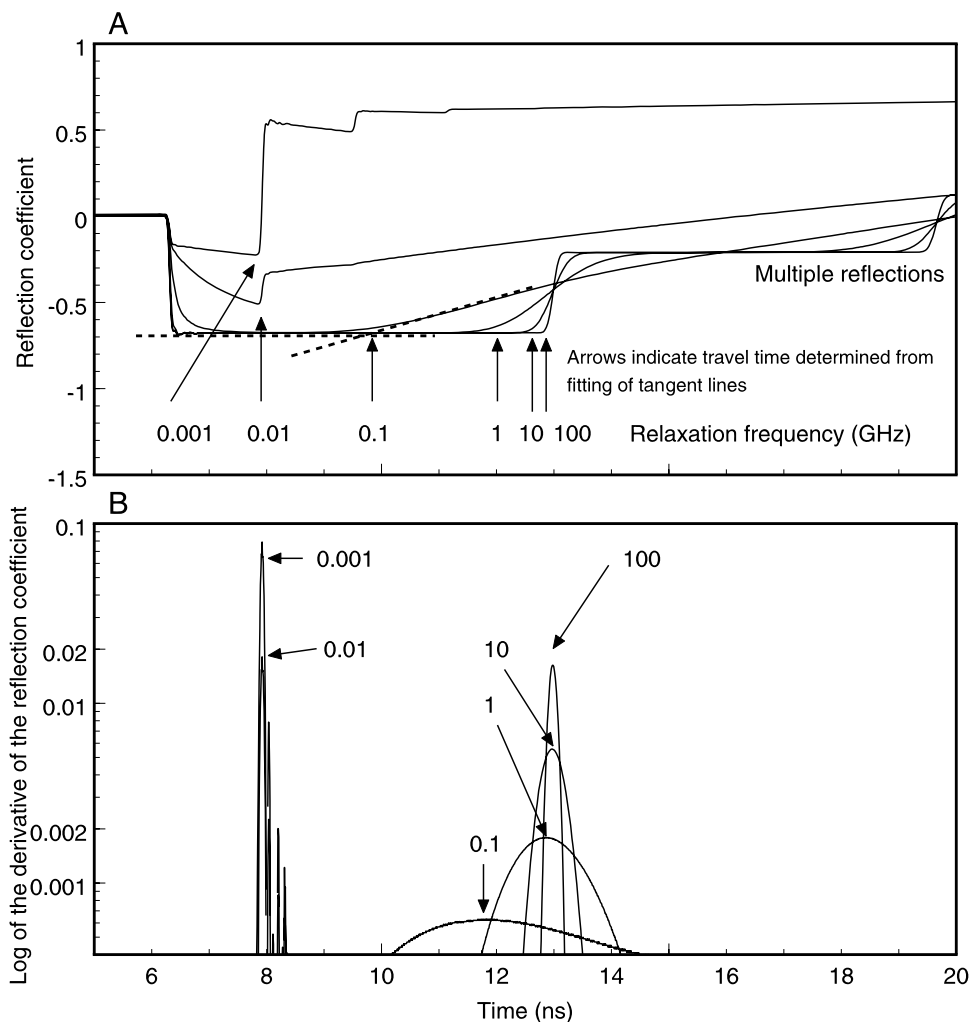


Figure 2. (a) Computer-generated waveforms illustrating how dispersion moving through the TDR bandwidth influences the shape of the TDR waveform. Relaxation frequencies vary from 0.001 to 100 GHz. (b) Derivatives of the waveforms in Figure 2a. The apex of the derivatives, corresponding with the maximum energy of the wave packet, are marked for the different relaxation frequency values. Multiple reflections have been removed from Figure 2b to increase clarity.

[17] Following the measurements using the TDR, the fluid mixture was poured into a beaker and a dielectric probe (Hewlett-Packard 85070B, Hewlett-Packard, Palo Alto, CA) inserted. The dielectric probe was connected to a network analyzer (Hewlett-Packard 8753B, Hewlett-Packard, Palo Alto, CA) allowing measurement of the real and imaginary permittivity between 300 kHz and 3 GHz. From these measurements, the effective frequency calculated from the TDR waveforms, could be used to obtain the corresponding real and imaginary permittivity from the frequency domain.

4. Results and Discussion

[18] Figure 2 presents results showing the impact of dispersion on TDR waveforms with different relaxation frequencies moving through the TDR signal bandwidth. Figure 2a illustrates the waveforms corresponding with the changing relaxation frequency. When the relaxation frequency of the material is 100 GHz a sharp TDR waveform is obtained. As the relaxation frequency reduces to 10 GHz

and 1 GHz a rounding of the reflected signal can be observed (location 10, 1 and 0.1, Figure 2a). This rounding of the reflected signal has important consequences as the tangent lines used to determine permittivity are observed to move to the left; tangent lines are fitted to the waveform with a relaxation at 0.1 GHz as an example. The tangent line intersection point is located at the point that the signal is first reflected, and represents the fastest traveling part of the signal; equivalent to the phase velocity. When the relaxation frequency is lower than 0.01 GHz the TDR signal responds mostly to the high-frequency permittivity (5.85). In Figure 2b the derivative of the time domain signal is presented. When the signal is viewed like this, the area under the derivative represents the relative energy content of the signal compared to its input value. In a nondispersive medium the phase and group velocity of the signal are similar, small differences may occur due to the presence of connectors etc. In a dispersive, nonconductive medium, the phase and group velocity diverge with the phase velocity traveling faster through the medium.

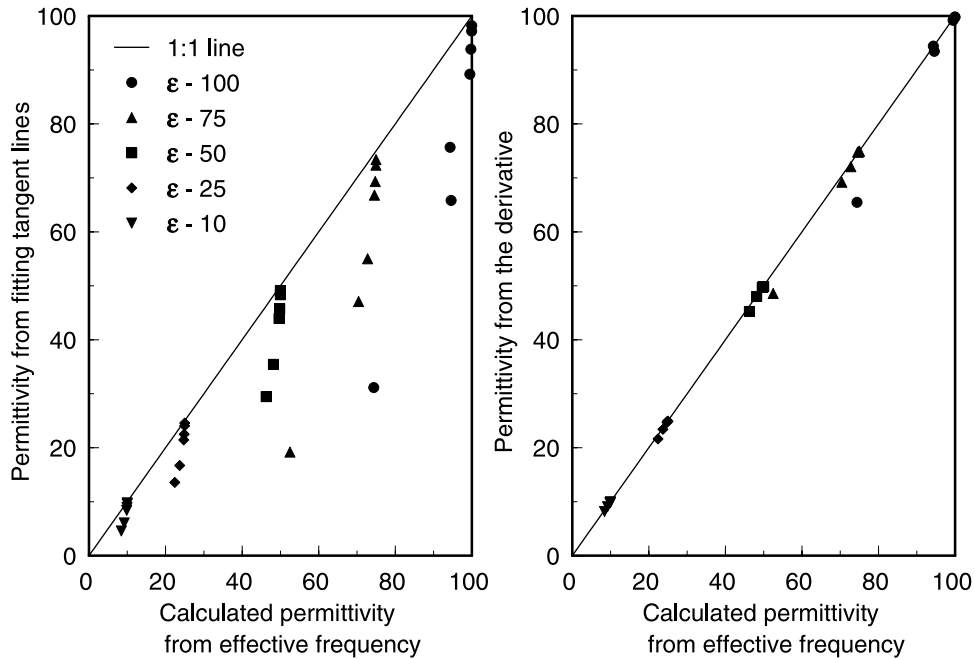


Figure 3. Results from the procedure described in Figure 1. Apparent permittivity (K_a) calculated from the effective frequency according to equation (3) is plotted on the x axis. (left) Apparent permittivity against the permittivity determined from travel time analysis using the tangent line fitting procedure (K_{aTAN}). (right) Permittivity determined using the derivative of the waveform procedure (K_{aDER}). It is clear that under dielectrically dispersive conditions (i.e., no conductive losses), effective frequency determined using the procedure described in equation (1) agrees with the permittivity determined with the derivative (K_{aDER}) and not with the permittivity from the ordinary tangent line fitting procedure (K_{aTAN}).

[19] Analysis of the 55 waveforms gave values for f_{eff} , and two values of apparent permittivity. One determined from fitting tangent lines K_{aTAN} , and the other from the apex of the derivative K_{aDER} . The value of f_{eff} could not be determined for waveforms with relaxation under 0.1 GHz as the multiple reflections merge leaving the first reflection indistinguishable from multiple reflections. Once frequency values are obtained from the waveform, the corresponding real and imaginary permittivities could be obtained from the appropriate Debye function. This allowed the calculation of an apparent permittivity value, K_a , using equation (3), which was taken to be the appropriate K_a value corresponding to f_{eff} determined from risetime. The results for K_{aTAN} , and K_{aDER} , plotted against the apparent permittivity determined from equation (3) are presented in Figure 3, the line represents the 1:1 line which the data should fall on if matching. Figure 3 clearly demonstrates that the permittivity calculated corresponding to the effective frequency with the permittivity determined from the apex of the derivative K_{aDER} .

[20] The mixtures of 1-propanol and water are used to verify the procedure used to determine the effective frequency for real measurements. The measured dielectric spectra for water, 1-propanol and mixtures 4 and 8 (Table 1) are presented in Figure 4; the corresponding waveforms are shown underneath. The procedure described in 3.1 was followed using the measured data; effective frequency was calculated from risetime, and used to determine the real and imaginary permittivity measured in the frequency domain using the network analyzer. An apparent permittivity, $K_{a(net. an.)}$ was calculated from these results using

equation (3), these were then compared to K_{aTAN} and K_{aDER} . The good correspondence of K_{aDER} to $K_{a(net. an.)}$ is evidenced in Table 1 by the low chi-square statistic (χ^2) shown for K_{aDER} as compared with the order of magnitude increase in χ^2 determined from tangent line fitting K_{aTAN} . The permittivity measured using the tangent line method corresponds to a higher frequency not determinable using the risetime methodology. What is encouraging from this analysis is that K_{aDER} gives a value of permittivity very close to the real permittivity, the imaginary permittivity appearing to have little effect on the travel time determination for values of ϵ'' up to 5.

[21] Having established that the effective frequency determined from risetime and K_{aDER} are compatible we present permittivity measured using K_{aDER} versus effective frequency (equation (1)) for a range of nondispersive and dispersive dielectric media in Figure 5. Measurements using fluids with no dispersion in the TDR bandwidth are shown with solid circles. The effective frequency as a function of permittivity for these materials in this probe design corresponds to the empirical model presented on the graph:

$$f_{eff} = e^{\left(6.35 + \frac{0.982}{\sqrt{\epsilon'}}\right)} \quad (14)$$

This provides an approximate value for the effective frequency to be expected for TDR measurements in nondispersive media for low-loss TDR probes. As the permittivity increases so the effective frequency is reduced; this model does not represent a universal relationship but will differ

Table 1. Results From Network Analyzer and TDR Measurements in 1-propanol/Water Mixtures^a

Fluid	Mixture Number	Mix Ratio	Risetime t_r , ns	f_{eff} MHz	ϵ'	ϵ''	$K_{a(\text{net. An.})}$	$K_{a\text{DER}}$	$K_{a\text{TAN}}$
Air		100	0.227	1540	1.0	0.0	1		
Water		100	0.554	632	78.1	2.5	78.7		
1-propanol/water	1	100	1.527	229	22.0	0.9	22.3	18.3	12.8
1-propanol/water	2	8:92	1.202	291	23.1	4.8	24.2	22.2	17.6
1-propanol/water	3	15:85	1.072	327	25.7	4.2	26.7	25.2	21.1
1-propanol/water	4	21:79	0.974	359	29.3	4.2	30.3	29.7	25.0
1-propanol/water	5	26:74	0.893	392	31.8	4.4	32.9	31.7	28.0
1-propanol/water	6	31:69	0.861	407	34.5	3.8	35.4	35.0	30.9
1-propanol/water	7	35:65	0.877	399	37.1	3.7	38.0	36.8	33.7
1-propanol/water	8	40:60	0.747	468	40.3	4.2	41.3	40.6	36.5
1-propanol/water	9	46:54	0.698	501	44.0	4.4	45.1	44.0	40.8
Chi-square								1.1	11.9

^aThe real (ϵ') and imaginary (ϵ'') permittivities were determined from network analyzer measurements, while the effective permittivities, K_a , were determined from the waveform. The predicted permittivity, $K_{a(\text{net. An.})}$, uses f_{eff} taken from the computed risetime and inserted into equation (3) along with the corresponding frequency-dependent ϵ' and ϵ'' values. Second reflections in the waveform computed using the apex of the derivative $K_{a\text{DER}}$ and by tangent line fitting $K_{a\text{TAN}}$ are also listed and compared using the chi-square statistic. The error associated with $K_{a\text{TAN}}$ is an order of magnitude larger than $K_{a\text{DER}}$.

according to each probe design. Measured waveforms can be more difficult to interpret than “clean”, computer-generated waveforms. This is due to impedance mismatches at the cable-probe head-probe interface and the filtering of higher frequencies. Results from measurements in nonconductive fluids indicate a maximum passable frequency of 1.54 GHz for this probe in air which is reduced to 0.632 GHz in water. Frequency reduction probably occurs due to some filtering of the high-frequency components of the signal because water has some relaxation in the TDR bandwidth. The open circles in Figure 5 represent the measurements made with bentonite; as the water content and hence permittivity and dispersion increase so the effective frequency reduces. This means in clay soils or clay bearing rocks with bentonite or other dispersive clays we would expect the effective frequency of the measurement to be reduced as the water content increased; perhaps to values as low as 100 or 200 MHz. In the case of both the alcohol water mixtures the opposite is demonstrated to be the case as the dispersion now reduces as the permittivity increases. Relaxation causes energy to be dissipated as heat, we believe that this primarily affects the higher frequencies first, so driving the effective frequency to lower values than in nonlossy dielectrics such as the acetone or water.

[22] These results, from both modeling and measurement clearly suggest that although equation (3) is a sine wave analogy for the step function, it provides an apparent permittivity value that corresponds with $K_{a\text{DER}}$ when effective frequency is determined from risetime. This work has not explored the impact of bulk electrical conductivity on the measurement; however as increasing EC attenuates and rounds the reflection this method is probably unsuitable in dielectric materials that have considerable bulk EC values. However, it does suggest that the method of determining effective frequency developed by J. A. Strickland (Time-domain reflectometry measurements, pp. 11–13, Tektronix Inc., Beaverton, Oregon, 1970) can be used for mildly dispersive dielectrics that have low losses in the TDR frequency band. This frequency value can be matched with $K_{a\text{DER}}$ determined using the travel time associated with the apex of the derivative of the waveform. This has a number of implications that are important for both probe design and

data interpretation. The frequency bandwidth of the signal for an individual TDR probe depends on the probe design and quality of construction. There is an upper limit to the frequency value that can be carried by the probe, what we

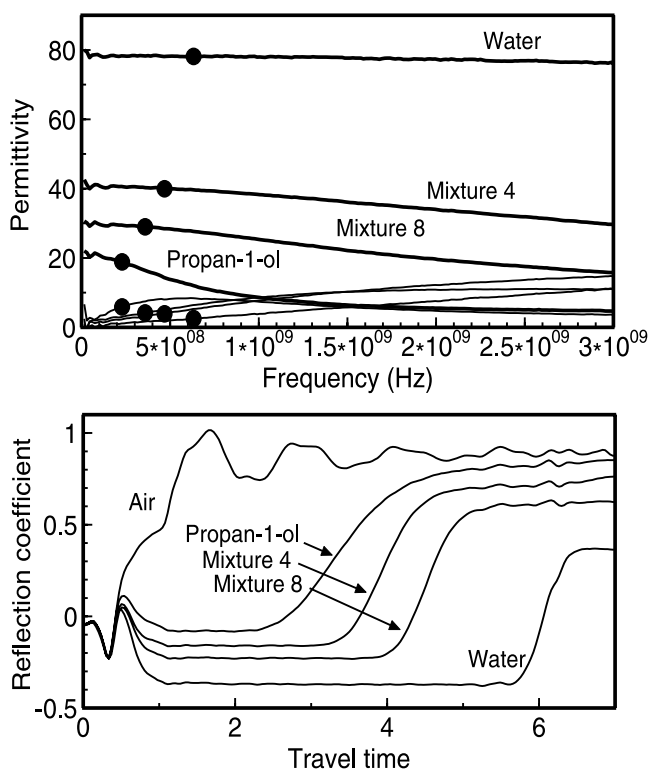


Figure 4. (top) Frequency-dependent permittivities measured with the network analyzer showing the real and imaginary permittivity of water, 1-propanol and mixtures 4 and 8 (Table 1). The circles are the effective frequencies determined from equation (1). (bottom) Waveforms collected using the TDR, which demonstrate the change in shape of the second reflection as the mixtures progress to pure 1-propanol, which has the greatest relaxation in the TDR bandwidth.

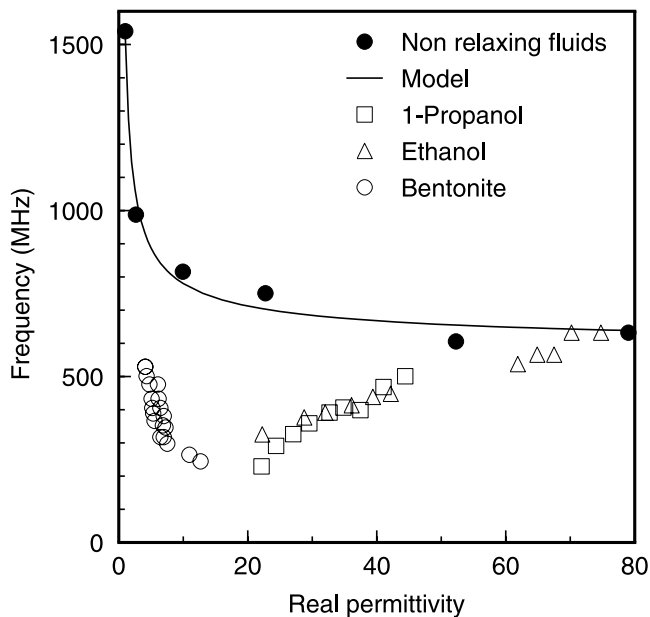


Figure 5. Effective frequencies determined for a range of dielectric materials. The solid circles describe materials with relaxations outside the TDR frequency bandwidth. They show an upper bound for effective frequency determined using the risetime method and are modeled using equation (14). The open circles are obtained from measurements in bentonite; as the water content increased and the permittivity was raised, the contribution of the dispersion became larger. Water contents of <0.3 were used to minimize any interference from bulk electrical conductivity. The ethanol and 1-propanol mixtures with water both show increasing permittivity with additional water where the imaginary permittivities were reduced and the effective frequencies increased.

term the maximum passable frequency. This should be determinable for any probe by placing it in a nondispersive dielectric such as air and determining the corresponding frequency from the risetime. Good quality construction of coaxial probes should lead to values of up to 1.75 GHz using a Tektronix 1502B with poorer probe design leading to the filtering of higher frequencies and values below 1 GHz. Cable length will also impact the dispersion with longer cables increasing the dispersion and signal risetime. We support the suggestion of *Hook et al.* [2004] that risetime is a good indicator of measurement quality and further suggest that it is also a good indicator of probe construction quality. The significance for data interpretation is that an estimate of the effective frequency for K_{aDER} can be made. This is useful for placing the measurement in the frequency domain where it might be compared with other measurements from either remote sensing devices or other instruments. Further work that explores the impact of bulk electrical conductivity on this measure will be a useful next step.

5. Summary and Conclusions

[23] We have presented results from TDR waveform modeling and measurements that were used to extract the apparent permittivity value that corresponds with the effective

frequency determined from the 10–90% risetime value. The modeling effort is based upon an equation for sine wave propagation of a signal along a transmission line used as an analogy for that of a step function. Results indicate that the apparent permittivity determined from the apex of the derivative of the waveform matches permittivity values corresponding to an effective frequency extracted from reflected signal risetime. The permittivity determined from tangent line analysis also has a frequency associated with it that is higher than the value determined from the 10–90% risetime value but not obtainable from this simple analysis. We term this value the maximum passable frequency and can be determined using the method of *Or and Rasmussen* [1999]. Results obtained from nondispersive media indicate that water content measurements in non dispersive soils will be expected to lie in the frequency range of 0.7–1.0 GHz. Measurements in bentonite indicate that the effective frequency is substantially reduced in this dispersive clay. In dielectrically dispersive clay soils effective frequencies will reduce as water content increases, perhaps to values as low as 100–200 MHz. The method of determining soil permittivity using the derivative of the waveform is suitable for nondispersive and dispersive media but is unlikely to work in electrically conductive soils such as saturated clays. The results also indicate the importance of high-quality probe construction and the importance of minimizing long cables. Higher frequencies are desirable for consistent water content measurements and will only be achieved through good probe design.

[24] **Acknowledgments.** The authors would like to acknowledge USDA NRI program grants (2002-35107-12507 and 2001-35107-11009) that made this work possible. M. Schaap was supported in part by the SAHRA Science and Technology Center at the University of Arizona under a grant from NSF (EAR-9876800).

References

- Chou Chang, F. R., N. T. Skipper, and G. Sposito (1995), Computer simulation of interlayer molecular structure in sodium montmorillonite hydrates, *Langmuir*, *11*, 2734–2741.
- Dean, T. J., J. P. Bell, and A. B. J. Baty (1987), Soil moisture measurement by an improved capacitance technique: I. Sensor design and performance, *J. Hydrol.*, *93*, 67–78.
- Debye, P. (1929), *Polar Molecules*, Dover, Mineola, N. Y.
- Dirksen, C., and S. Dasberg (1993), Improved calibration of time domain reflectometry soil water content measurements, *Soil Sci. Soc. Am. J.*, *57*, 660–667.
- Elmore, W. C., and M. A. Heald (1985), *Physics of Waves*, Dover, Mineola, N. Y.
- Feng, W., C. P. Lin, R. J. Deschamps, and V. P. Drnevich (1999), Theoretical model of a multisection time domain reflectometry measurement system, *Water Resour. Res.*, *35*, 2321–2331.
- Fernando, M. J., R. G. Bureau, and K. Arulanandan (1977), A new approach to determination of cation exchange capacity, *Soil Sci. Soc. Am. J.*, *41*, 818–820.
- Heimoavaara, T. J. (1994), Frequency domain analysis of time domain reflectometry waveforms: 1. Measurement of the complex dielectric permittivity of soils, *Water Resour. Res.*, *30*, 189–199.
- Heimoavaara, T. J., and E. de Water (1993), A computer controlled TDR system for measuring water content and bulk electrical conductivity of soils, *Rep. 41*, Lab. of Phys. Geogr. and Soil Sci., Univ. of Amsterdam, Amsterdam.
- Hilhorst, M. A. (1998), Dielectric characterisation of soil, *Publ. 98-01*, Inst. of Agric. and Environ. Eng. (IMAG-DLO), Wageningen, Netherlands.
- Hook, W. R., T. P. A. Ferre, and N. J. Livingston (2004), The effects of salinity on the accuracy and uncertainty of water content measurement, *Soil Sci. Soc. Am. J.*, *68*, 47–56.
- Huisman, J. A., A. H. Weerts, T. J. Heimoavaara, and W. Bouten (2002), Comparison of travel time analysis and inverse modeling for soil water

- content determinations with time domain reflectometry, *Water Resour. Res.*, 38(6), 1077, doi:10.1029/2001WR000259.
- Huisman, J. A., S. S. Hubbard, J. D. Redman, and A. P. Annan (2003), Measuring soil water content with ground penetrating radar: A review, *Vadose Zone J.*, 2, 476–491.
- Ibbotson, L. (1999), *The Fundamentals of Signal Transmission*, Edward Arnold, London.
- Kelleners, T. J., R. W. O. Soppe, D. A. Robinson, M. G. Schaap, J. E. Ayars, and T. H. Skaggs (2004), Calibration of capacitance probes using electric circuit theory, *Soil Sci. Soc. Am. J.*, 68, 430–439.
- McNairn, H., T. J. Pultz, and J. B. Boisvert (2002), Active microwave remote sensing methods, in *Methods of Soil Analysis*, part 4, *Physical Methods*, SSSA Book Ser., vol. 5, edited by J. H. Dane and G. C. Topp, pp. 475–488, Soil Sci. Soc. of Am., Madison, Wis.
- Or, D., and V. P. Rasmussen (1999), Effective frequency of TDR travel time based measurement of bulk dielectric permittivity, paper presented at Third Workshop on Electromagnetic Wave Interaction With Water and Moist Substances, Russell Agric. Res. Cent., Athens, Ga., 12–13 April.
- Paltineanu, I. C., and J. L. Starr (1997), Real-time water dynamics using multisensor capacitance probes: Laboratory capacitance probes, *Soil Sci. Soc. Am. J.*, 61, 1576–1585.
- Robinson, D. A., S. B. Jones, J. M. Wraith, D. Or, and S. P. Friedman (2003a), A review of advances in dielectric and electrical conductivity measurements in soils using time domain reflectometry, *Vadose Zone J.*, 2, 444–475.
- Robinson, D. A., M. G. Schaap, S. B. Jones, S. P. Friedman, and C. M. K. Gardner (2003b), Considerations for improving the accuracy of permittivity measurement using TDR: Air/water calibration, effects of cable length, *Soil Sci. Soc. Am. J.*, 67, 62–70.
- Schaap, M. G., D. A. Robinson, S. P. Friedman, and A. Lazar (2003), Measurement and modelling of the TDR signal propagation through layered dielectric media, *Soil Sci. Soc. Am. J.*, 67, 1113–1121.
- Sun, Z. J., G. D. Young, R. A. McFarlane, and B. M. Chambers (2000), The effect of soil electrical conductivity on moisture determination using time-domain reflectometry in sandy soil, *Can. J. Soil Sci.*, 80, 13–22.
- Topp, G. C., and P. A. Ferre (2002), Water content, in *Methods of Soil Analysis*, part 4, *Physical Methods*, SSSA Book Ser., vol. 5, edited by J. H. Dane and G. C. Topp, pp. 417–421, Soil Sci. Soc. of Am., Madison, Wis.
- Topp, G. C., J. L. Davies, and A. P. Annan (1980), Electromagnetic determination of soil water content: Measurements in coaxial transmission lines, *Water Resour. Res.*, 16, 574–582.
- Topp, G. C., S. Zegelin, and I. White (2000), Impact of real and imaginary components of relative permittivity on time domain reflectometry measurements in soils, *Soil Sci. Soc. Am. J.*, 64, 1244–1252.
- Von Hippel, A. R. (1954), *Dielectrics and Waves*, John Wiley, Hoboken, N. J.
- Wadell, B. C. (1991), *Transmission Line Design Handbook*, Artech House, Norwood, Mass.
- White, I., J. H. Knight, S. J. Zegelin, and G. C. Topp (1994), Comments on “Considerations on the use of time domain reflectometry (TDR) for measuring soil water content”, *Eur. J. Soil Sci.*, 45, 503–508.
-
- S. B. Jones and D. A. Robinson, Department of Plants, Soils and Biometeorology, Utah State University, Logan, UT 84322, USA. (darearthscience@yahoo.com)
- D. Or, Department of Civil and Environmental Engineering, University of Connecticut, Storrs, CT 06269, USA.
- M. G. Schaap, George E. Brown Jr. Salinity Laboratory, 450 W. Big Springs Road, Riverside, CA 92507, USA.